AUTHOR and OTHER-AUTHOR

[Left hand page running head is author's name in Times New Roman 8 point bold capitals, centred. For more than two authors, write **AUTHOR et al.**]

CONFERENCE PRE-PRINT

IMPACT OF THE TEMPERATURE RATIO ON TURBULENCE AND IMPURITY TRANSPORT IN THE EAST PLASMA CORE

G.S. Li

Institute of Plasma Physics, Chinese Academy of Sciences Hefei, People's Republic of China Email: gsli@ipp.ac.cn

T. Zhang, Z. Zhou, X.H. Wu, K.N. Geng, X.X. Zhang, K.D. Li, S.X. Wang, F. Wen, X.J. Liu, Y.J. Liu, S.T. Mao, W.M. Zhang, L. Zhang, H.Q. Liu, G.Q. Li, X. Gao and the EAST team Institute of Plasma Physics, Chinese Academy of Sciences Hefei, People's Republic of China

Z. Xu

School of Electrical and Optoelectronic Engineering, West Anhui University Luan, People's Republic of China

Abstract

Controlling impurity content in tokamaks is crucial for both safe device operation and optimal plasma performance. Therefore, it is of significant value to study impurity turbulent transport mechanisms under conditions relevant to future reactors, which will feature reduced collision rates and toroidal rotation. A dedicated experiment was conducted on EAST, a tokamak with a fully metallic wall, to study turbulent impurity transport processes in electron-heating-dominated plasmas. This was achieved by adjusting the electron-to-ion temperature ratio (Te/Ti) to regulate turbulence levels, with identical amounts of argon impurity injected at different Te/Ti plateaus. The results show that argon impurity seeding can suppress ion heat transport driven by ITG and TEM modes, thereby contributing to increased ion temperature. Simultaneously, the diffusion coefficient and convection velocity of argon are both dominated by the turbulent component. Furthermore, in the case with Te/Ti closer to unity, the core ITG turbulence intensity is lower, resulting in the minimum amount of argon impurity being transported to and accumulated in the plasma core. These findings reveal a clear picture of the interactions between turbulence behavior and impurity transport in electron-heating-dominated plasma cores. We believe this work provides support for ITER's new baseline.

1. INTRODUCTION

The switch from beryllium (Be) to tungsten (W) for the first wall of ITER's new baseline makes it crucial to study the transport behavior of high-Z impurities and their effects on plasma performance in electron-heating-dominated plasmas. Under ITER-like conditions, the impact of high-Z impurities can be assessed through the injection of low-Z impurities such as argon. The alpha particles generated by fusion initially heat the electrons, which then transfer energy to ions through collisions, leading to a typically higher electron temperature than ion temperature. As energy transfer continues, the electron-to-ion temperature ratio (Te/Ti) gradually approaches 1 and eventually stabilizes between 1 and 2 [1]. Variations in this temperature ratio can excite microscopic instabilities at ion and electron scales in the plasma core through different mechanisms, triggering competition and coupling among various modes, thereby altering turbulent transport behavior [2]. Turbulent transport is believed to dominate impurity dynamics in the plasma core. In future reactors, reduced collision rates and toroidal rotation are expected to further enhance the dominance of turbulent effects [3]. Therefore, systematically investigating turbulent characteristics in the plasma core under future fusion reactor conditions (Te/Ti close to unity) and elucidating the regulatory mechanisms of turbulence on impurity transport are of significant importance for evaluating and predicting the performance targets of future devices such as ITER and DEMO, as well as for developing effective impurity control strategies.

The EAST device, with its ITER-like full-metal wall structure and flexible electron heating capabilities, provides an exceptional experimental platform for conducting relevant research [4]. A dedicated experiment was performed on EAST to study the turbulent impurity transport processes in the plasma core by adjusting the temperature ratio to regulate the turbulence level. The paper is organized as follows. Section 2 describes the experimental setup and observations on EAST. Section 3 presents the integrated modeling conducted within the OMFIT framework to explain the experimental observations. First, the TGLF code was used to analyze the effect of argon impurity injection on micro-instabilities and the consequent increase in ion temperature. Subsequently, TGYRO analyses were employed to examine how different temperature ratio regimes result in variations of argon transport

properties, which in turn lead to differences in the degree of ion temperature enhancement. Finally, section 4 summarizes the results.

2. EXPERIMENTAL SETUP AND OBSERVATIONS

2.1. Experimental setup

EAST is a fully superconducting tokamak with a fully metallic wall. Its key parameters include a major radius (R) of ~1.9 m, a minor radius (a) of ~0.45 m, a toroidal magnetic field of up to 2.6 T, and a plasma current of up to 1 MA. In this work, a series of experiments were performed on a 400 kA current platform with a 2.4 T toroidal magnetic field. Figure 1 below shows the experimental setup for three typical discharges. The three discharges share similar waveforms, with 2 MW NBI serving as the background heating, and the plasma density is feedbackcontrolled at an identical level to mitigate the effects of rotation and density peaking. Here, EC heating power is adjusted to different power levels to modulate the central electron-ion temperature ratio, thus producing varying degrees of turbulence in the plasma core. Equal amounts of a mixture of 50% Ar and 50% D₂ are injected by gas puffing from the lower divertor at different EC heating power levels, as shown in Figure 2. In discharges #139946, #139949, and #139955, argon impurity was injected at t = 4.2 s, 5.2 s, and 5.2 s, with corresponding electron cyclotron (EC) heating powers of 2.85 MW, 2.35 MW, and 1.8 MW, respectively. Following a short delay after argon injection, the plasma exhibits significant evolution (as indicated by the shaded region): a rise in the effective charge number (Zeff), toroidal rotation velocity, core ion temperature, and line-averaged density, contrasted by a gradual drop in core electron temperature. This leads to a reduction in plasma stored energy. However, a comparison among the three discharges reveals divergent levels of change in Zeff and enhancement in ion temperature. This indicates that the underlying complex interactions between turbulence and impurities following the Ar injection are distinct across these discharges.

The key plasma profiles were measured by a suite of diagnostics, as illustrated in Figure 2. The electron temperature was obtained from a multichannel electron cyclotron emission (ECE) diagnostic. Ion temperature and toroidal rotation velocity (Vt) profiles in the core region ($\rho = 0$ –0.6) were measured by a tangential x-ray crystal spectrometer (TXCS). The density profile was measured by a fast-sweeping density profile reflectometer (DPR). The line-averaged density $\langle n_e \rangle$ was provided by the core channel polarimeter-interferometer (POINT). Here, ρ is defined as the square root of the normalized toroidal flux, and this work primarily focuses on the plasma core region ($0 < \rho < 0.6$).

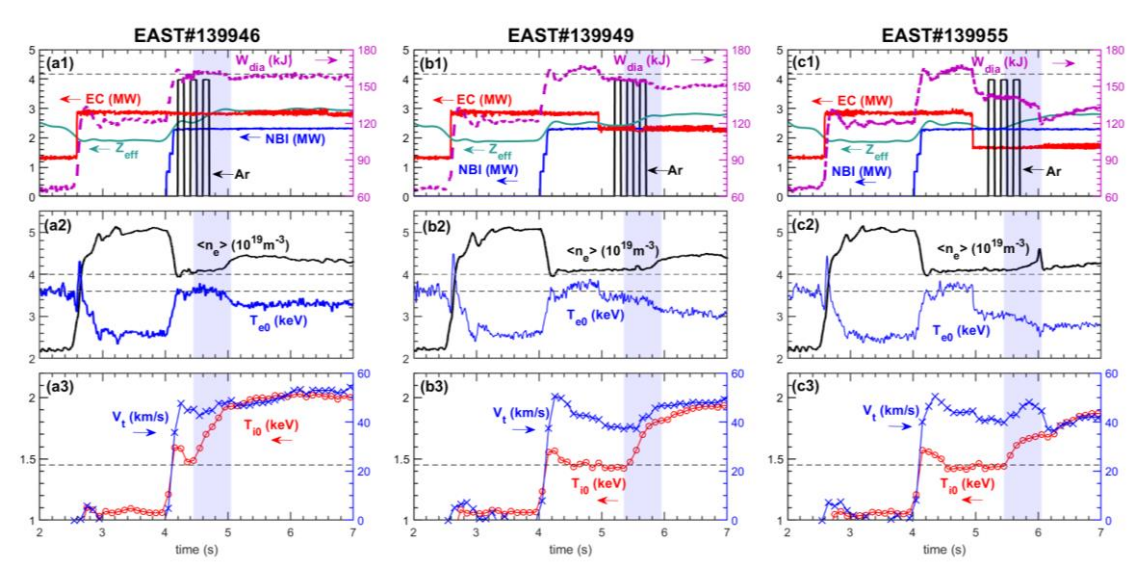


FIG. 1. Experimental setup. Three discharges have the similar waveform, but different EC power.

[Left hand page running head is author's name in Times New Roman 8 point bold capitals, centred. For more than two authors, write

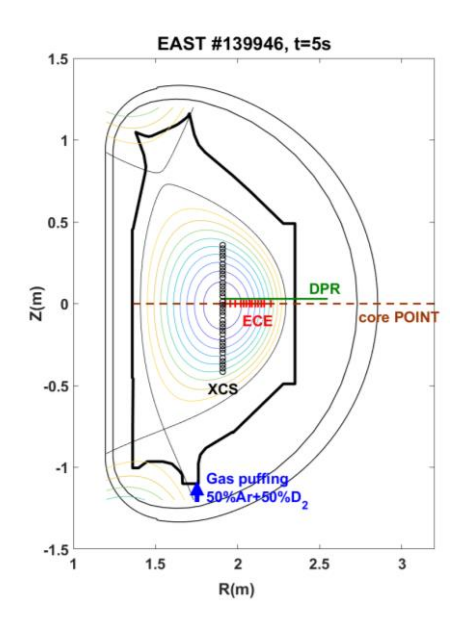


FIG. 2. The poloidal cross-section of EAST device and the diagnostics utilized in this work.

2.2. Experimental observation

To clearly illustrate the modifications induced by argon impurity injection, discharge #139949 was selected for detailed analysis. Figure 3 displays two-dimensional contour plots of electron density, electron temperature, ion temperature, and toroidal rotation velocity over the time interval t=4-7 s. Following argon injection at t=5.2 s, the plasma begins to undergo significant changes from approximately t=5.5 s. A marked increase in toroidal rotation velocity is observed within the region of $\rho < 0.45$. The ion temperature rises across the inner region of $\rho < 0.5$, with the most pronounced enhancement localized to the core at $\rho < 0.3$. In contrast, the electron temperature exhibits a gradual decay across the entire profile. Regarding electron density, a gradual increase is observed inside $\rho < 0.92$, which is consistent with the rising line-averaged density shown in panels a2, b2, and c2 of Figure 1. It is important to note that while pedestal behavior can significantly influence impurity transport, the position of the density pedestal (indicated by the black contour near $\rho = 0.92$) shows no notable shift before and after the injection. This observation suggests that the effect of pedestal dynamics on impurity transport can be considered negligible in this analysis.

For a comparative analysis, two characteristic time slices were selected from each of the three discharges: State 'A', defined as the moment just after argon injection but before the onset of significant plasma modification; and State 'B', representing a later time when the plasma had reached a relatively stable phase following the impurity-induced changes. The chosen time points are $t=4.3\ s$ (State A) and $4.9\ s$ (State B) for #139946; $t=5.3\ s$ (State A) and $5.9\ s$ (State B) for #139949 and #139955. The corresponding profiles are compared in Figure 4. Analysis of the State A profiles reveals that while the density and ion temperature profiles are similar across the three discharges, the electron temperature and toroidal rotation velocity profiles exhibit a distinct step-like transition. Specifically, a gradual decrease is observed across the entire core region (0 < ρ < 0.6) from #139946 to #139949 and then to #139955 at their respective State A time points. This progression effectively establishes a platform for studying turbulent transport under varying temperature ratios. In the State B profiles, elevations are observed in the electron density, ion temperature, and rotation profiles, whereas the electron temperature shows no significant systematic change.

A notable finding is the differing degree of ion temperature enhancement following argon injection across the three discharges. To facilitate comparison, the time axes for these discharges were aligned to their respective injection times (to), as shown in Figure 5. Prior to injection, the core electron-to-ion temperature ratio (T_c/T_i) differs significantly among them, decreasing sequentially from #139946 to #139949 to #139955. Furthermore, during the impurity-induced transition, this temperature ratio decreases in all cases, suggesting a modification of core turbulence properties. Crucially, the magnitude of ion temperature enhancement also diminishes sequentially from #139946 to #139955. This variation in ion temperature enhancement is strongly correlated with the concentration of impurities in the plasma core. Within a certain range, a higher impurity concentration correlates with a greater increase in ion temperature. Our results therefore indicate that the argon concentration in the core

decreases from #139946 to #139949 to #139955, a conclusion further supported by the correspondingly smaller increases in the effective charge number (Zeff). This finding demonstrates a clear dependence of both impurity content and turbulence levels on the temperature ratio. The underlying physics of this correlation will be detailed in Section 3 through simulation analysis.

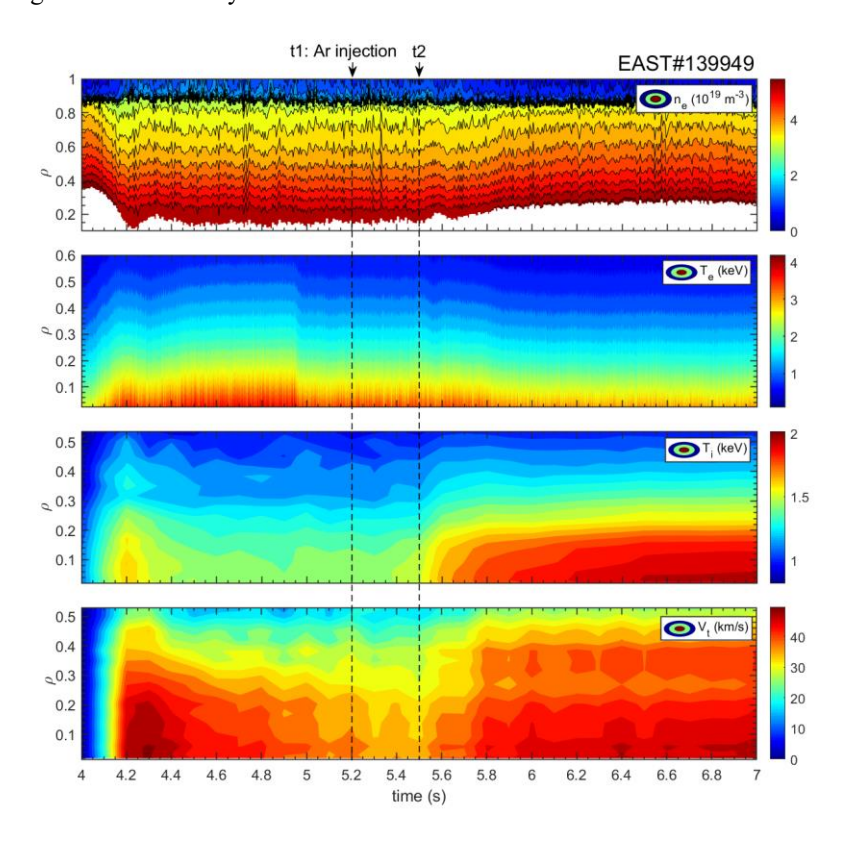


FIG. 3. The time evolution of electron density, electron temperature, ion temperature, and rotation velocity during argon impurity injection.

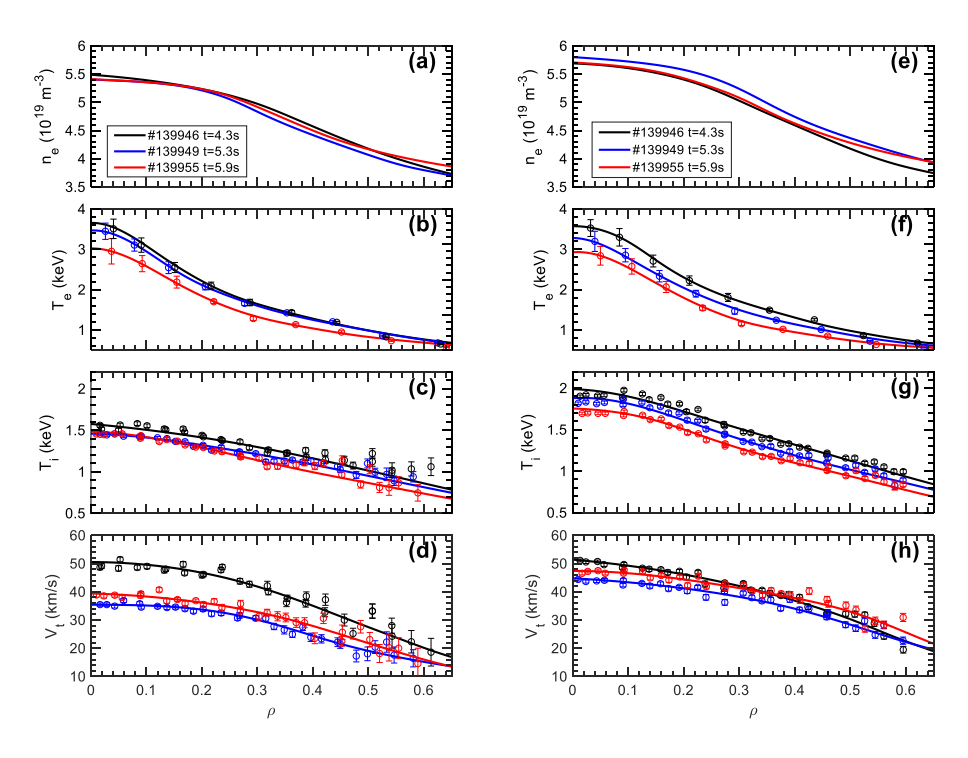


FIG. 4. Comparison of profiles before and after argon impurity injection. Panels (a)-(d) show the pre-injection phase, and panels (e)-(h) show the post-injection phase.

[Left hand page running head is author's name in Times New Roman 8 point bold capitals, centred. For more than two authors, write AUTHOR et al.]

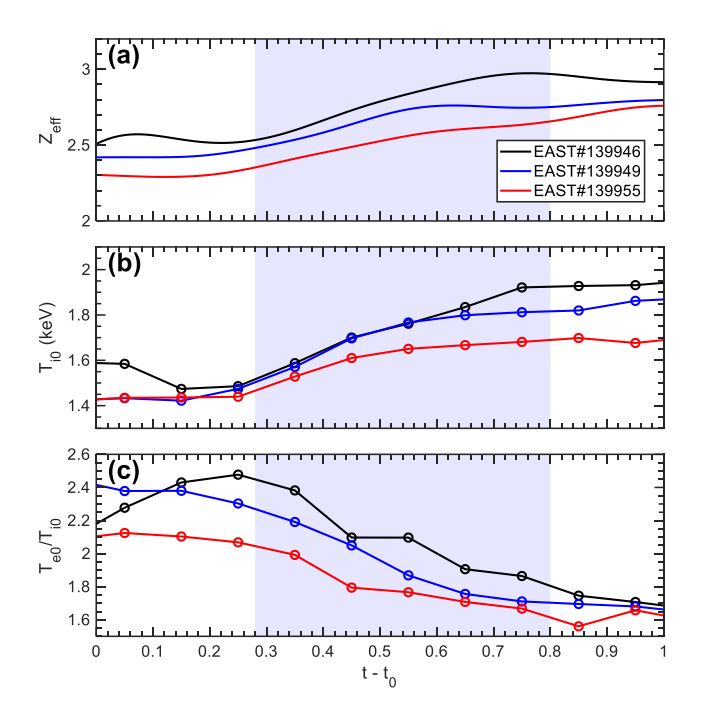


FIG. 5. Comparison of the time evolution of temperature ratio (Te₀/Ti₀), core ion temperature (Ti₀), and the effective charge number (Zeff) during argon impurity injection. The time axes for the three discharges have been aligned at the impurity injection time for comparison.

3. SIMULATION ANALYSIS

3.1 Effect of Argon Impurity Injection on Micro-instabilities and Confinement

The micro-instabilities in the plasma core are analyzed using the gyro-Landau-fluid model TGLF [5], which utilizes the fitted profiles from Figure 4 as input. The dominant micro-instabilities observed in the tokamak plasma core are the low-k mode ($k_y < 1$), which includes the ion temperature gradient (ITG) mode and the trapped electron (TEM) mode, and the high-k mode ($k_y > 1$) electron temperature gradient (ETG) mode [6]. Here, $k_y = k_\theta \rho_s$, where k_θ is the poloidal wavenumber, $\rho_s = C_s/\Omega_s$, $C_s = \sqrt{T_e/m_i}$, and $\Omega_s = eB/(m_i c)$. Figures 6-8 present the TGLF-calculated ky spectrum of the most unstable mode, along with the corresponding normalized linear growth rate ($\gamma' = \gamma(a/Cs)$) and frequency ($\alpha' = \omega(a/Cs)$), for three discharges. The length scale α is the circular equivalent minor radius of the last closed flux surface. The upper panels display γ' , and the lower panels display α' for the most unstable modes, respectively. A positive value of the frequency α' indicates that the mode rotates in the electron diamagnetic direction, corresponding to ETG or TEM. Conversely, a negative value indicates ITG. These most unstable modes can thus be identified by combining the k_y spectra of growth rate and frequency. The TGLF results reveal distinct instability characteristics among the three plasmas.

Panels (a) and (c) of Figures 6, 7, and 8 present the TGLF calculation results for the time after argon impurity injection but just before the plasma transition (i.e., State A described in Section 2.2). It can be observed that for all three time points, the low-k turbulence is dominated by TEM in the core region and by ITG further out (near 0.4 < rho < 0.6). However, the spatial extent and growth rates of these instabilities differ slightly across the three time points. Notably, the growth rate of ITG is significantly higher than that of TEM. The high-k turbulence, driven by ETG, spans the entire spatial range. It should be noted that, compared to ITG and TEM, the impact of ETG on impurity transport is negligible due to its smaller spatial scale; therefore, this paper focuses primarily on the changes in ITG and TEM. Panels (b) and (d) of Figures 6, 7, and 8 show the TGLF results for the time after argon impurity injection when the plasma reached a relatively stable phase (i.e., State B in Section 2.2). Compared to State A, the turbulence spectra in State B for all three time points show that the spatial extent of TEM shrinks and its growth rate decreases. Meanwhile, the spatial extent of ITG expands and shifts inward toward the core. However, the growth rate of ITG is significantly reduced within the $0.4 < \rho < 0.6$ region. This analysis indicates that the increase in ion temperature is primarily due to the suppression of ion heat transport, which is driven by the reduced growth rates of both TEM and ITG.

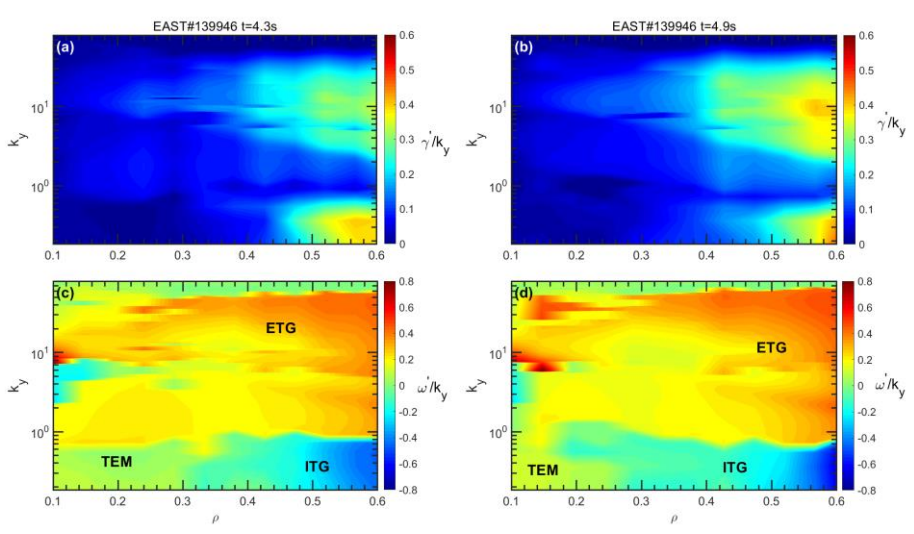


FIG. 6. Turbulence spectra in the plasma core ($0 < \rho < 0.6$) from TGLF simulations for discharge #139946. (a, b) Normalized growth rates and (c, d) normalized frequencies at t=4.3 s (before Ar injection) and t=4.9 s (after Ar injection).

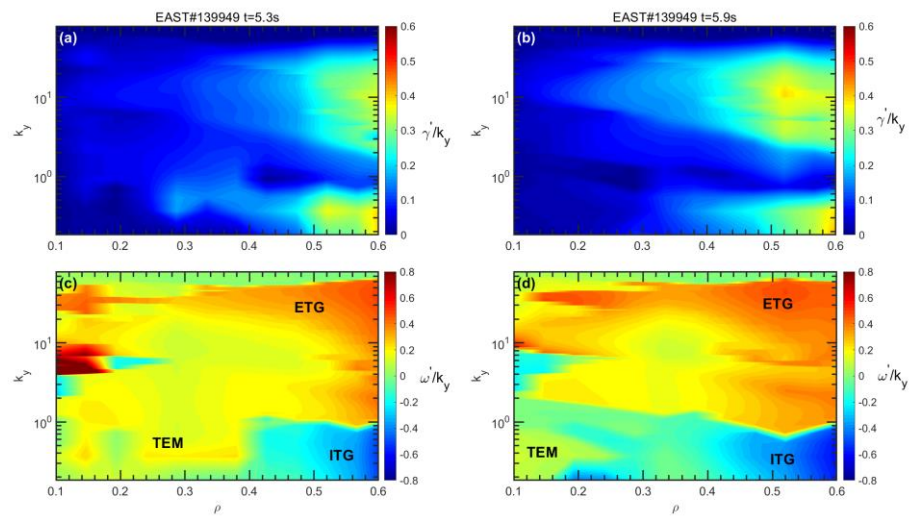


FIG. 7. Turbulence spectra in the plasma core ($0 < \rho < 0.6$) from TGLF simulations for discharge #139949. (a, b) Normalized growth rates and (c, d) normalized frequencies at t = 5.3 s (before Ar injection) and t = 5.9 s (after Ar injection).

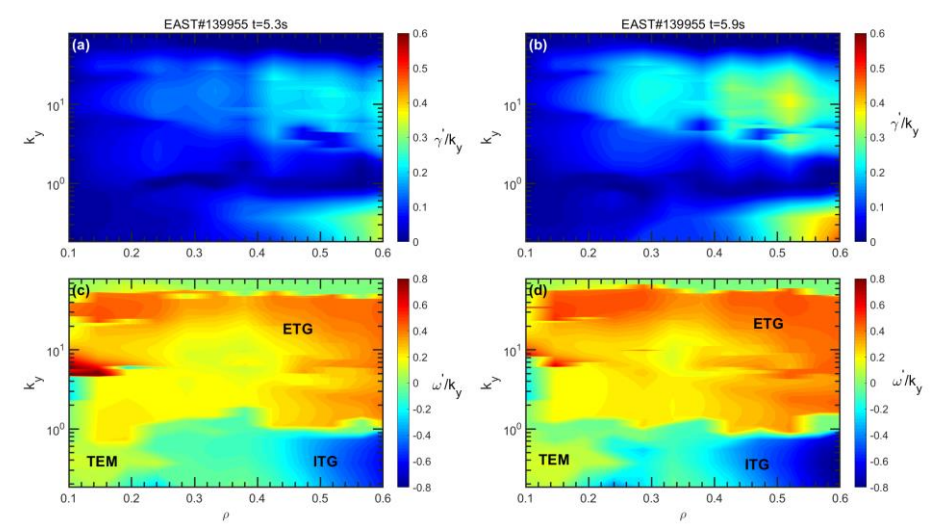


FIG. 8. Turbulence spectra in the plasma core $(0 < \rho < 0.6)$ from TGLF simulations for discharge #139955. (a, b) Normalized growth rates and (c, d) normalized frequencies at t=5.3 s (before Ar injection) and t=5.9 s (after Ar injection).

[Left hand page running head is author's name in Times New Roman 8 point bold capitals, centred. For more than two authors, write **AUTHOR et al.**]

3.2 Impact of Turbulence on Argon Transport and Concentration

To analyze the impact of turbulence on argon impurity transport and content, we first compared the growth rates of the most unstable modes at different radial positions ($\rho = 0.19, 0.28, 0.38, 0.47,$ and 0.56) for discharges #139946 (t=4.3s), #139949 (t=5.3s), and #139955 (t=5.3s). The growth rate was found to increases from the core (ρ =0.19) toward the edge (ρ =0.56), with the value at ρ =0.56 being approximately ten times higher than that at ρ =0.19. Consequently, turbulence in the region of ρ =0.47–0.56 is expected to play the dominant role in transport. A comparison of the turbulence modes and growth rates at ρ =0.47 and ρ =0.56 for the three discharges, we found that the turbulence is primarily driven by the ITG mode in all cases. The highest growth rate is observed in #139946 (t=4.3s), followed by #139949 (t=5.3s), with the smallest in #139955 (t=5.3s). This indicates a sequential reduction in ITG-driven turbulence intensity from shot to shot, which would enhance the turbulent contribution to impurity transport.

Subsequently, we analyzed the transport characteristics of Ar XV (Argon 15+) for these three time slices using TGYRO, a method whose application to impurity transport calculations has been well documented in [7]. The results show that for all three cases, the turbulent component dominates both the Ar diffusion coefficient and the convection velocity. The turbulent terms for #139949 (t=5.3s) and #139955 (t=5.3s) are comparable and significantly higher than that for #139946 (t=4.3s). The ratio V/D shown in Figs. 10(c1), (c2), and (c3) is negative in all cases, indicating inward impurity transport. The V/D profile for #139955 (t=5.3s) is slightly smaller than those for the other two discharges. Given that V/D is proportional to the impurity density gradient, a smaller V/D implies less impurity peaking. This suggests that the core Ar impurity content is lowest in #139955 (t=5.3s). Consequently, the increase in core ion temperature and the change in Zeff are the smallest for this discharge, a finding consistent with the experimental observations presented in Section 2.2.

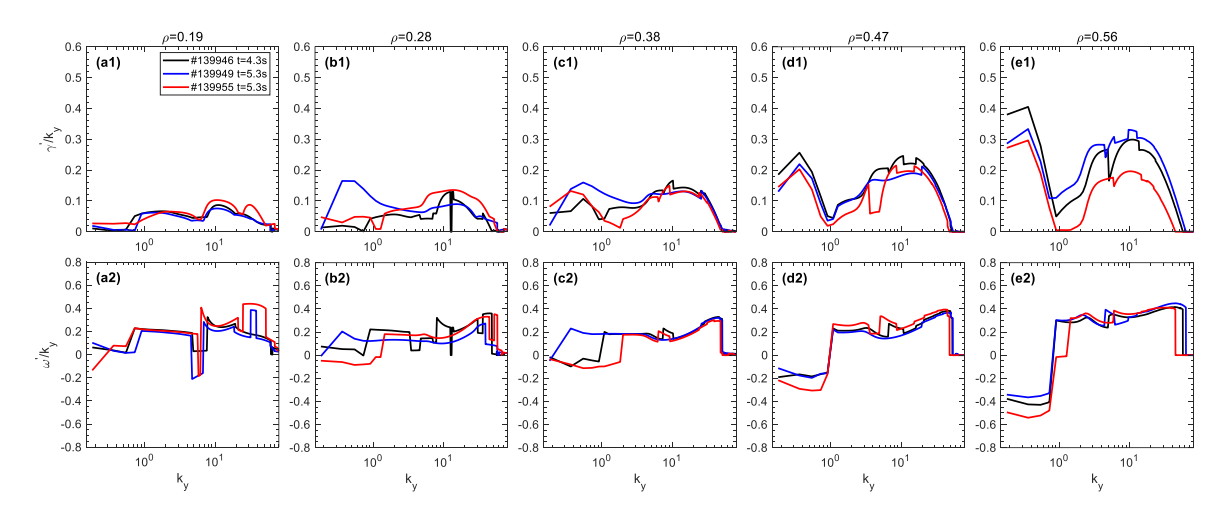


FIG. 9. Growth rate and frequency of the most unstable modes at radial positions $\rho = 0.19, 0.28, 0.38, 0.47,$ and 0.56 for discharges: #139946 (t=4.3s), #139949 (t=5.3s), and #139955 (t=5.3s).

4. SUMMARY

This work presents a dedicated experiment conducted on the EAST device to investigate turbulent impurity transport processes in the plasma core. The experimental approach involved adjusting the electron-to-ion temperature ratio (Te/Ti) to establish distinct turbulence levels, during which identical amounts of argon impurity were injected. A comparative analysis of the argon-induced modifications to plasma confinement across these different regimes was performed to systematically study the interplay between impurities and turbulence. The results demonstrate that argon impurity seeding suppresses the micro-instabilities that dominate plasma heat transport, thereby enhancing the ion temperature. Conversely, these same micro-instabilities drive impurity transport, which regulates the core argon density and leads to variations in the achieved ion temperature improvement. Furthermore, this work reveals the characteristics of core turbulence and turbulent impurity transport under reactor-relevant conditions with Te/Ti close to unity, providing important insights for evaluating and predicting the performance of future fusion devices.

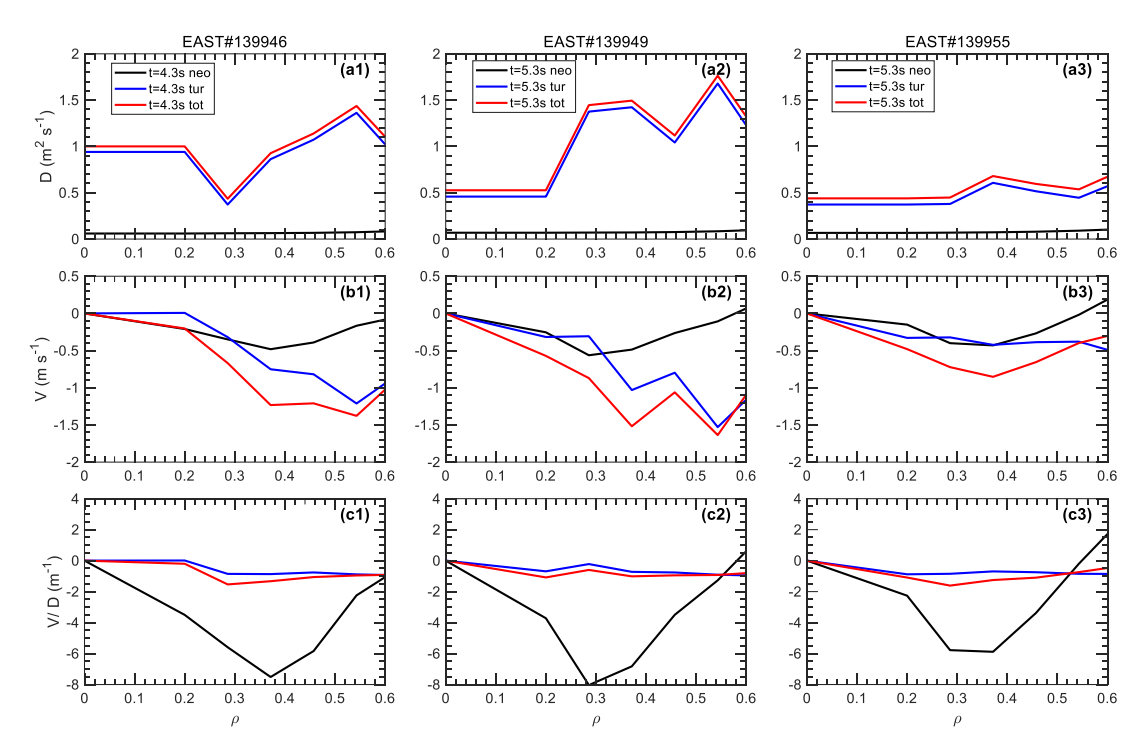


FIG. 10. Transport characteristics of Ar XV (Argon 15+) in discharges: #139946 (t=4.3s), #139949 (t=5.3s), and #139955 (t=5.3s).

5. REFERENCES

- [1] Maeyama, Shinya et al Nature communications 13.1 (2022): 3166.
- [2] Alessandro Casati et al Phys. Plasmas 15, 042310 (2008)
- [3] M. Yoshida et al 2025 Nucl. Fusion 65 033001
- [4] J.G. Li et al Engineering 7 (2021) 1523
- [5] G. M. Staebler et al Phys. Plasmas 12, 102508 (2005)
- [6] A. Mariani et al 2019 Nucl. Fusion 59 126017
- [7] O. Meneghini et al 2021 Nucl. Fusion 61 026006